

# Growth, structural and mechanical characterization and reliability of chemical vapor deposited Co and Co<sub>3</sub>O<sub>4</sub> thin films as candidate materials for sensing applications

V. P. TSIKOURKITOUDI, E. P. KOUMOULOS, N. PAPADOPOULOS<sup>a</sup>, E. HRISTOFOROU<sup>a</sup>, C. A. CHARITIDIS\*  
*National Technical University of Athens, School of Chemical Engineering, 9 Heroon Polytechniou Str., Zografos, Athens, Greece GR-157 80*

<sup>a</sup>*National Technical University of Athens, School of Mining Engineering and Metallurgy, 9 Heroon Polytechniou Str., Zografos, Athens, Greece GR-157 80*

The adhesion and mechanical stability of thin film coatings on substrates is increasingly becoming a key issue in device reliability as magnetic and storage technology driven products demand smaller, thinner and more complex functional coatings. In the present study, chemical vapor deposited Co and Co<sub>3</sub>O<sub>4</sub> thin films on SiO<sub>2</sub> and Si substrates are produced, respectively. Chemical vapor deposition is the most widely used deposition technique which produces thin films well adherent to the substrate. Co and Co<sub>3</sub>O<sub>4</sub> thin films can be used in innovative applications such as magnetic sensors, data storage devices and protective layers. The surface topography of the produced thin films is investigated with Atomic Force Microscopy and the mechanical behavior of them is evaluated. The produced thin films are also characterized using nanoindentation technique. Typical load-displacement curves are obtained and the local changes observed are explained. The nanomechanical properties (hardness and elastic modulus) of the thin films are obtained with Oliver & Pharr model. Finally, an evaluation of the reliability of each thin film (wear analysis) is performed using the hardness to elastic modulus ratio in correlation to the ratio of irreversible work to total work for a complete loading-unloading procedure.

(Received January 25, 2012; accepted February 20, 2012)

*Keywords:* Chemical Vapor Deposition, Co thin films, Co<sub>3</sub>O<sub>4</sub> thin films, Nanoindentation, Nanomechanical Properties

## 1. Introduction

Experimental and theoretical studies of the properties of metal thin films on semiconductive surfaces have been stimulated by their fundamental and practical importance in the field of surface science, materials research and technology [1, 2]. In the recent years, the deposition of Co on Si substrates has attracted special interest, as Co thin films can be used in innovative magnetic devices in microelectronics, allowing their incorporation in Si technology and rendering them as candidate materials for sensing and data storage applications. Co<sub>3</sub>O<sub>4</sub> thin films are also promising candidates due to useful properties, such as high catalytic activity at low cost [3], antiferromagnetism [4] and electrochromism [5] and have been considered for uses as magnetic detectors, counter electrodes, humidity or oxygen optical sensors [6], solar-selective absorbers and protective layers [7].

Chemical vapor deposition remains the most widely used deposition technique in many fields, especially for depositing thin films of electronic materials. It is capable of producing highly dense films with good adhesion to the substrate [8].

To our best knowledge, little research has been performed on the mechanical properties of Co and Co<sub>3</sub>O<sub>4</sub> thin films for sensing applications. Thus, the mechanical characterization of Co and Co<sub>3</sub>O<sub>4</sub> thin films is worth being

studied and is prerequisite in order that the aforementioned thin films to be used as structural/functional elements in devices applications. The mechanical behavior of magnetic and storage devices is important in understanding reliability issues and concerns; mechanical and tribological aspects are of critical importance in determining long-term stability of such devices. Creep behavior is also another important issue which affects the reliability of the aforementioned devices [9]. Since many magnetic and sensing devices are often composed of multiple layers of thin films, the development of residual intrinsic stresses is possible during the microfabrication process. Such stresses are generated due to crystal dislocations, grain boundary interactions, excess vacancies or phase transformations and can provoke rupture and/or delamination of the thin film layer affecting the long-term stability and reliability of the aforementioned devices. For this reason, an appropriate control of intrinsic stresses is needed in order to ensure the commercialization and reliable operation of magnetic and sensing devices. Recently, nanoindentation has proven to be a powerful technique in providing information on mechanical properties (hardness,  $H$ , and elastic modulus,  $E$ ) of thin films, based on analysis of load-displacement curves. Nanoindentation has attracted increasing interest, since allows a reliable characterization contrary to traditional methods i.e. micro hardness and

tensile test [10]. The shape of the load-displacement curves differ from one material to another and these differences usually indicate different mechanical properties. Significant interest has been shown on possible local changes, such as discontinuities and perturbations, observed on the load-displacement curves, as they may be a signal of physical events beneath the indenter, characterized by absorb or release of energy [11]. Such local changes may indicate the aforementioned causes of the generation of intrinsic stresses.

In the present research study, the surface topography of chemical vapor deposited Co and  $\text{Co}_3\text{O}_4$  thin films is investigated through Atomic Force Microscopy (AFM) analysis and their magnetic behavior is evaluated. Furthermore, the nanomechanical properties of the aforementioned thin films are obtained through nanoindentation technique. An analysis of the local changes observed on the load-displacement curves of Co and  $\text{Co}_3\text{O}_4$  thin films is also among the scopes of the present study. Finally, an analysis based on the  $H/E^*$  ratio is performed in order to estimate the wear resistance of the thin films.

## 2. Experimental

The films were grown in a vertical, cylindrical MOCVD stainless steel reactor [12], specifically developed for the deposition of magnetic films, either singled or multilayered. The reactor had computer controlled switching of gases for abrupt transients during deposition of multilayered structures. It also employed two independent precursor lines and four separate gas delivery lines for maintaining inert, (He or Ar), reductive ( $\text{H}_2$ ) or oxidizing ( $\text{O}_2$ ) atmosphere. Prior to reactor's entrance heat traced lines were used.

The substrates were positioned onto a stainless steel block, with three 4' recessed pockets. The three zone resistance heating was controlled by Ch-Al thermocouples embedded at the block's bottom surface with PID controllers. Two rotary vane pumps in-line connected were used for reactor's evacuation down to a base pressure of  $10^{-4}$  mbar and process pumping accurately controlled by a manual throttle valve.

Silicon and blanket silicon dioxide were used as substrates. These were ex situ cleaned by a 30-sec Piranha etch solution, and then by a subsequent acetone and methanol rinse. Finally, they were washed with double-distilled water followed by drying in a high purity Ar atmosphere. In the case of the silicon substrates an additional first step was employed. These were dipped for 1 min in a 10% solution of HF acid and were immediately rinsed by double-distilled water.

The Co films were deposited from a cobalt carbonyl precursor. The latter was introduced to the reactor as an aerosol mixture, formed by the dissolution of cobalt carbonyl into dichloromethane, 0.1 M concentrated. In a typical experiment a liquid (solution) flow of 7 g/h was mixed with a hydrogen gas flow of 0.05 l/min at 27 °C.

The mixture (aerosol) was then introduced to the reactor, the temperature of which had been adjusted to 140 °C.

In a typical experiment of  $\text{Co}_3\text{O}_4$  deposition [13] the substrates were loaded and the reactor was purged with an argon flow of 0.75 l/h, while the susceptor was heated to the desired temperature (450 °C). Then a solid inclusion complex (placed in a specialized glass reservoir) of  $\beta$ -cyclodextrin with  $\text{CoI}_2$  was sublimed at 115 °C [14], and the vapors were introduced into the reactor with the aid of a constant  $\text{O}_2$  flow of 50 ml/min.

The thickness of the produced films is 150 nm.

AFM was used to provide additional information regarding films' surface topography and geometrical complexity. Imaging of the surface morphology was performed using a 'Quesant – Qscope 250'. The AFM was equipped with a 40  $\mu\text{m}$  Dual PZT scanner. High-resolution images were obtained at different areas at the maximum scanning rate of 6 Hz and with 600 X 600 pixels resolution. All AFM images were acquired in ambient conditions at the intermittent contact mode. The scanned surfaces were also characterized by the surface roughness histograms. The magnetic response data were obtained by vibrating sample magnetometry with the aid of a VSM 155 Princeton Applied Research (2T). An external magnetic field was applied either parallel or normal to the film's surface.

The nanoindentation tests in this work were performed using a nanomechanical test instrument, equipped with a Berkovich tip (120 nm tip radius) which allows the application of loads from 1 to 10000  $\mu\text{N}$ . The instrument is capable of recording penetration displacements as a function of applied loads with a high load resolution (1 nN) and a high displacement resolution (0.04 nm). The above instrument is equipped with a Scanning Probe Microscope (SPM), in which the sharp probe tip moves in a raster scan pattern across a sample surface using a three-axis piezo positioner. In all depth-sensing tests, a total of 10 indents were averaged to determine the mean  $H$  and  $E$  values for statistical purposes, with a spacing of 50  $\mu\text{m}$  (~45% relative humidity, 23°C). Prior to indentation, the area function of the indenter tip was calibrated in a fused silica, a standard material for this purpose.

## 3. Results and discussion

**Surface Topography.** The  $\text{Co}_3\text{O}_4$  films were uniformly grain distributed with, however enlarged grains (Fig. 1a), probably due to high deposition temperature. As was proved by histogram analysis (Fig. 1b) the mean surface roughness (RMS) deviation of the films deposited at 450 °C was of the order of 5.5 nm, with the mean height being around 17.5 nm. On the contrary, the Co films originating from  $\text{Co}_2(\text{CO})_8$  presented an extremely smooth surface (Fig. 2a) with a mean surface roughness around 2 nm and an average height of about 12.5 nm, as was revealed by histogram analysis (Fig. 2b).

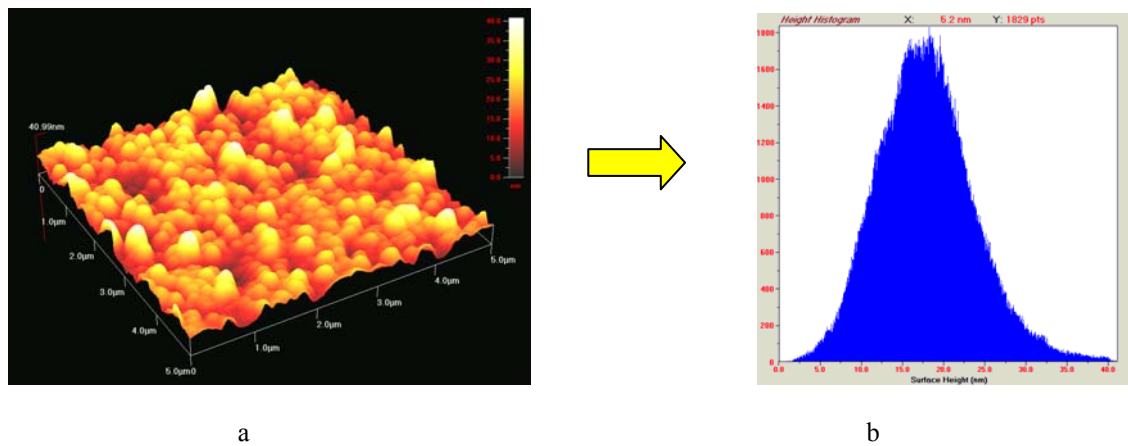


Fig. 1. AFM (a) and histogram analysis (b) of Co<sub>3</sub>O<sub>4</sub> thin films, respectively.

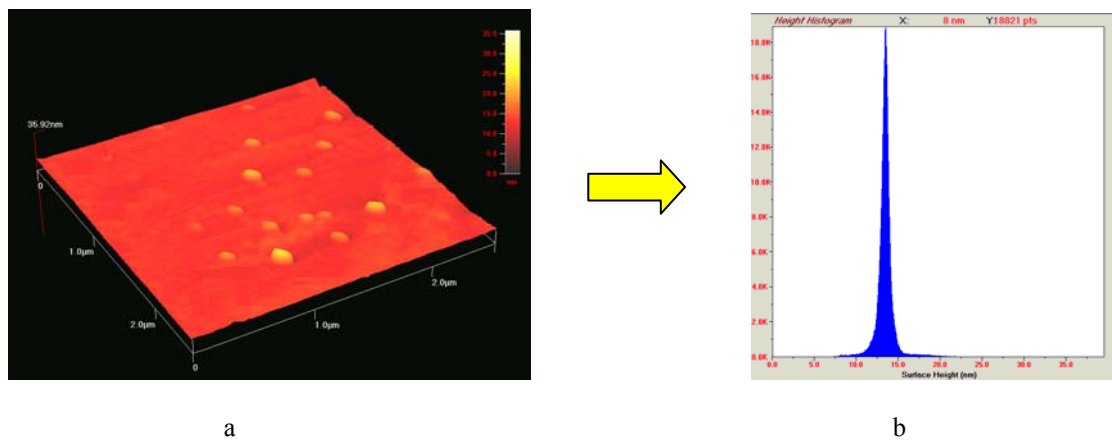


Fig. 2. AFM (a) and histogram analysis (b) of Co thin films, respectively.

**Magnetic properties.** The magnetic responses of both Co<sub>3</sub>O<sub>4</sub> and Co films under an externally applied magnetic field are presented in Fig. 3 (a-b). It was found that the easy axis of magnetization was the films' plane. The anisotropy field was found around 480 kA/m and 800

kA/m, respectively. Large anisotropy fields were recorded, especially for the Co films produced by Co<sub>2</sub>(CO)<sub>8</sub>. The coercive field along the hard axis magnetization was below the sensitivity limits of our magnetometer.

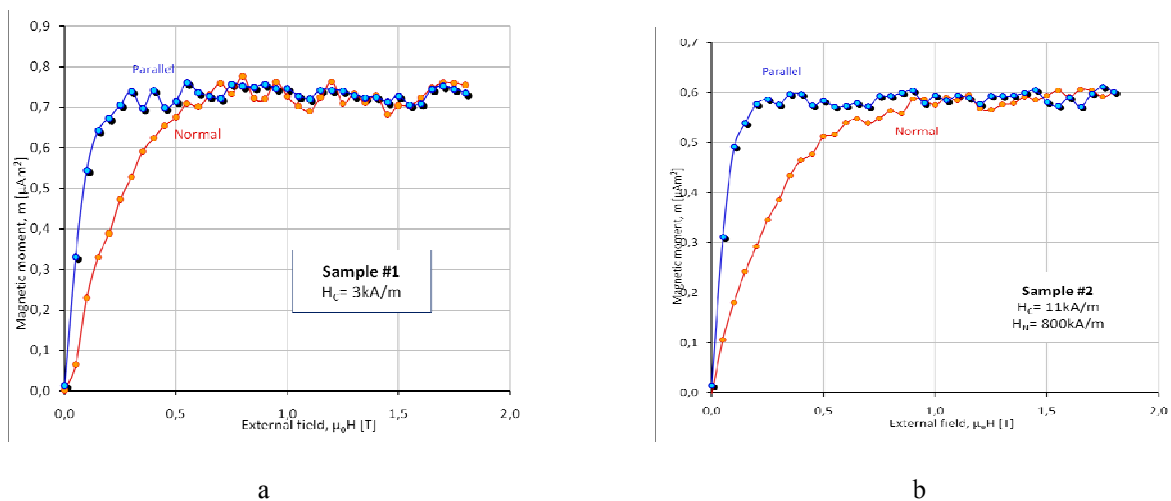


Fig. 3. Magnetic responses of Co<sub>3</sub>O<sub>4</sub> (a) and Co (b) thin films, respectively.

**Load-displacement Curves.** The loading-unloading curves of the probed materials are presented in Fig. 4 (a-b) (comparison for applied loads of 500 and 1000  $\mu\text{N}$ ).  $\text{Co}_3\text{O}_4$  thin film exhibits higher resistance to applied load, i.e. higher applied load values are needed in order to reach the same displacement (higher values of hardness). In the case of Co, greater plasticity is revealed, i.e. energy stored at the material after the indentation is over (total integration of curve area).

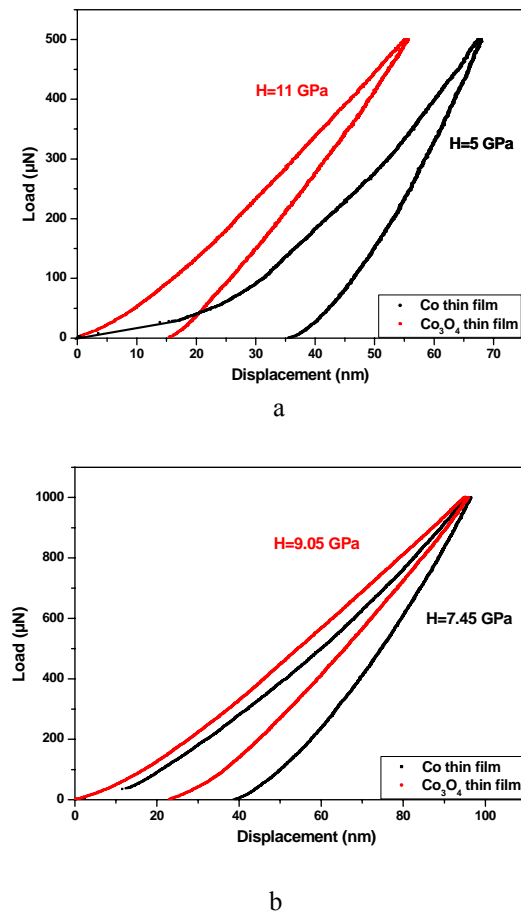


Fig. 4. Loading-unloading curves of Co and  $\text{Co}_3\text{O}_4$  thin films (applied loads 500(a) & 1000(b)  $\mu\text{N}$ ).

In Fig. 5 (a-b), typical load-displacement curves of Co and  $\text{Co}_3\text{O}_4$  thin films are presented showing local changes (discontinuities), i.e. changes in the slope, referred as pop-ins and elbows in the loading and in the unloading curve, respectively. During the pop-in, the indenter tip penetrates in the sample without an increase in the applied load. The first pop-in in each sample reveals the onset of plasticity, i.e. the first point at which plastic yield occurs. The onset of plasticity occurs at  $\sim 10$  nm for each thin film. In this stage, the nanoindenter can be approximated as spherical and the experimental data deviate from the fully elastic curve. For lower loads than the load where the onset of plasticity occurs, reversibility of the indentations performed is observed. The pop-ins indicate a redistribution of material around the indentation site

(activity of atoms beneath the indenter). This is observed when a dislocation source is activated (first pop-in), is moving and multiplying (for pop-ins observed at higher loads) [11]. Several studies [15] propose that phase transformation and formation of cracks at the interface between the thin film and the interface may also contribute to pop-ins. As it is obvious from the representative load-displacement curves presented in Fig. 5(a-b), a large number pop-ins appear during nanoindentation of Co thin film.

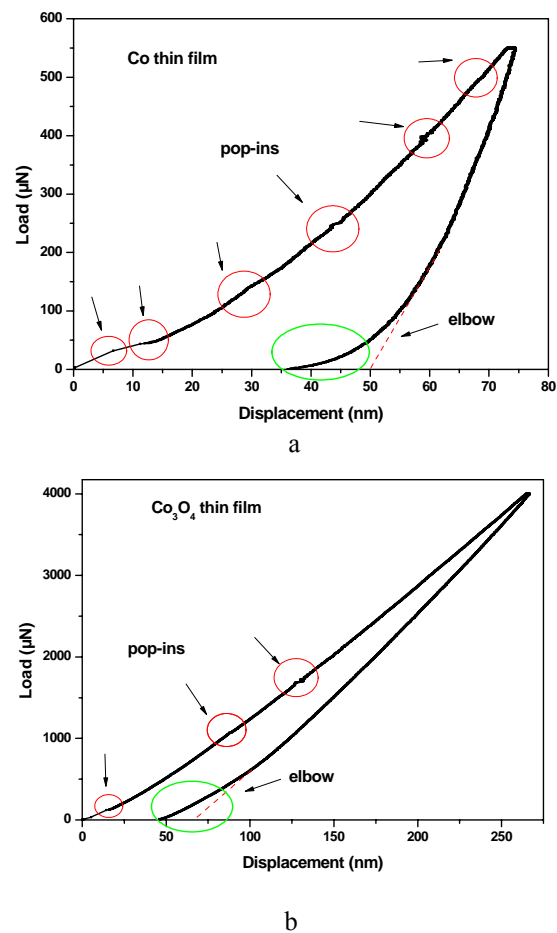


Fig. 5. Typical load-displacement curves of Co (a) and  $\text{Co}_3\text{O}_4$  (b) thin films showing pop-ins and elbow.

Apart from the pop-ins in the loading curve, a change in slope (“elbow”) is also observed in the unloading curves of Fig. 5 (a-b) (green circles). This linear unloading observed as an elbow may indicate the buckling of the thin film in order that the exerted compressive load is relieved. For this reason, the buckled material may rise and push back on the indenter [16]. The elbow can also be associated with phase transformations [17].

**Nanomechanical Properties.** At each imposed displacement, the true indentation  $E$  and the  $H$  can be deduced from the curves using the Oliver & Pharr model (O&P) [18], which calculates the contact area between the indenter tip and the sample using the tangent of the upper

part (30%) of the unloading curve, which is considered to be linear, along with the known area function. In *O&P* model, the derived expressions for calculating the elastic modulus from indentation experiments are based on Sneddon's elastic contact theory [19] (Equation 1):

$$E_r = \frac{S\sqrt{\pi}}{2\beta\sqrt{A_c}} \quad (1)$$

where  $S$  is the unloading stiffness (initial slope of the unloading load-displacement curve at the maximum displacement),  $A_c$  is the projected contact area between the tip and the substrate and  $\beta$  is a constant that depends on the geometry of the indenter ( $\beta=1.167$  for Berkovich tip). Conventional nanoindentation hardness refers to the mean contact pressure, which depends on the geometry of the indenter (Eq. 2):

$$H_c = \frac{F}{A} \quad (2)$$

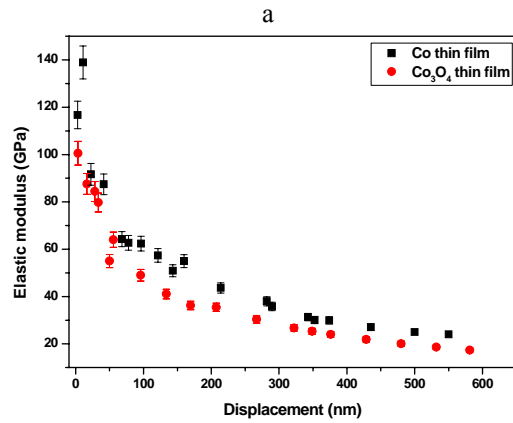
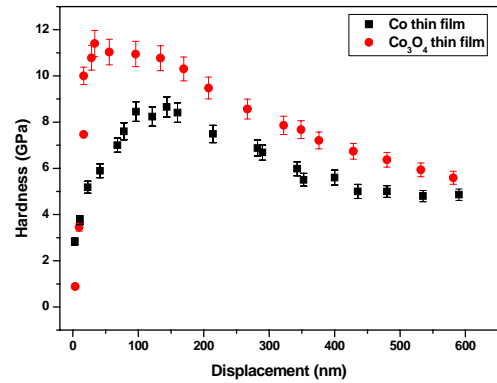
The graphs in Figs.6a & 6b show the mean value of the  $H$  and  $E$  measurements as a function of the imposed displacement (the trend of the curvatures is similar for all samples). As the indentation displacement increases below 100 nm, a small increase of the  $H$  values is observed (Fig. 6a). This increase is probably a combination of either thin film nanomechanical properties, real effect of a native oxide at the surface and an artifact of the shape of the indenter tip for shallow displacements [10, 20-21]. As far as the  $E$  values are concerned (Fig. 6b), they are similar for the two thin films. The obtained results for  $H$  and  $E$  values are in good agreement with similar measurements presented in the literature, as presented in Table 1.

Table 1. Hardness and Elastic Modulus values of Co thin films as presented in the literature and this work..

| $H$ (GPa)        | $E$ (GPa)     | Displacement (nm) | Reference |
|------------------|---------------|-------------------|-----------|
| between 8 and 10 | not mentioned | ~150              | [22]      |
| 4.25             | 85.15         | -                 | [23]      |
| 8.65             | 54.97         | 150               | this work |

**Instant hardness analysis.** According to contact mechanics, the instant hardness (measured at maximum displacement) during loading can be calculated as a function of the displacement or load. As shown in Figure 7, Co<sub>3</sub>O<sub>4</sub> thin film exhibits enhanced resistance (with almost twice the hardness in 40 nm of displacement, arrow-noted) to deformation (instant hardness) compared to Co thin film, for identical loading rate. It is reported that the instant hardness changes over a wide range of the indentation loads tested [24]. Considering that hardness is defined as the material's resistance to plastic deformation loaded by an indenter, it is determined by the average contact pressure when the material responds plastically.

When the material exhibits plastic hardening behavior, the contact pressure will change with the indentation applied load [25]. After the transition from elastic to plastic deformation, no hardening is shown in Fig. 7, revealing that  $H$  remains unchanged (also shown in Fig. 6)



b

Fig. 6. Hardness (a) and elastic modulus (b) values as a function of the displacement of the indenter.

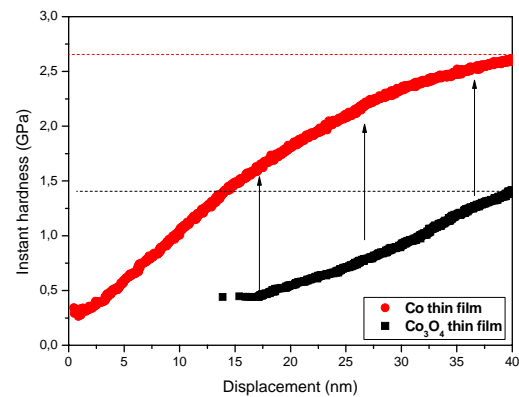


Fig. 7. The instant hardness as a function of displacement both Co<sub>3</sub>O<sub>4</sub> and Co thin films (extracted from Fig. 4a).

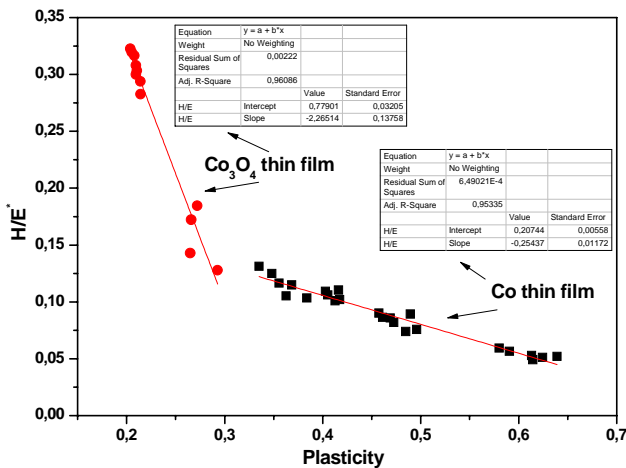


Fig. 8. Linear correlation of  $H/E^*$  and  $(W_{tot} - W_u)/W_{tot}$  for both  $Co_3O_4$  and Co thin films.

**Hardness to Modulus Ratio–Wear Analysis.** The total work created by the indenter ( $W_{tot}$ ) which causes elastoplastic deformation at a maximum displacement and the work transferred by the sample to the indenter during unloading ( $W_u$ ), have been examined. It was found that a remarkable correlation exists between the ratio of irreversible work to total work for a complete loading-unloading procedure,  $(W_{tot} - W_u)/W_{tot}$ , and the  $H/E^*$  term [25] is given below (Eq. 3):

$$\frac{H}{E^*} = \Pi_{\theta} \frac{(W_{tot} - W_u)}{W_{tot}}, \quad (3)$$

where  $E^* = E/(1 - \nu^2)$ . The subscript,  $\theta$ , denotes a possible dependence on indenter angle. Fig. 8 shows that for a given indenter angle, there is an approximate linear relationship between  $H/E^*$  and  $(W_{tot} - W_u)/W_{tot}$ . The  $Co_3O_4$  thin film exhibits higher resistance to wear, compared with Co thin film. Nanoscratch testing of the samples revealed identical behaviour ( $Co_3O_4$  thin film presented lower coefficient of friction). Thus, the material used in each application should be carefully chosen, depending on the demands of the application. Consequently, the value  $H/E^*$  may be obtained from the measurement of  $W_u$  and  $W_{tot}$ , which can be calculated from simple numerical integration based on load and displacement measurements.

The  $H/E^*$  ratio is of significant interest in tribology. This ratio multiplied by a geometric factor is the ‘plasticity index’ which describes the deformation properties of rough surfaces [26]. The correlation provides an alternative method for measuring  $H/E^*$  on micro- and nano- scale for both metals and ceramics. Furthermore, both  $H$  and  $E^*$  may be obtained using the above correlation together with a well-known relationship between  $E$ , contact area, and initial unloading slope [25, 27].

## 4. Conclusions

Chemical vapor deposited Co and  $Co_3O_4$  thin films on  $SiO_2$  and Si, respectively, were produced and characterized. The AFM analysis revealed that the  $Co_3O_4$  films are uniformly grain distributed with enlarged grains (mean roughness  $\sim 17.5$  nm), whereas the Co films originating from  $Co_2(CO)_8$  presented an extremely smooth surface (mean surface roughness  $\sim 2$  nm). As far as the magnetic responses of both  $Co_3O_4$  and Co films under an externally applied magnetic field, it was found that the easy axis of magnetization was the films’ plane. The anisotropy field was found around 480 kA/m and 800 kA/m, respectively. The load-displacement curves obtained from the nanoindentation technique showed that the  $Co_3O_4$  thin film exhibited higher resistance to applied load (i.e. higher applied load values are needed in order to reach the same displacement). In the case of Co, greater plasticity was revealed, i.e. energy stored at the material after the indentation was over. An investigation of the local changes presented on the load-displacement curves was performed, revealing that the onset of plasticity for both thin films was at  $\sim 10$  nm. Furthermore, it was found that the  $Co_3O_4$  thin film was more resistant and stable under the exertion of load. The nanomechanical properties ( $H$  and  $E$ ) for displacement 150 nm ( $H=8.65$  GPa &  $E=54.97$  GPa,) were found to be in good agreement with the literature. Finally, a wear analysis was performed using the  $H/E^*$  ratio in correlation to the  $(W_{tot} - W_u)/W_{tot}$  term. The  $Co_3O_4$  thin film exhibited higher resistance to wear, compared with Co thin film. Thus, depending on the demands of the application, the material used should be carefully chosen.

## Acknowledgements

The authors wish to acknowledge NTUA funded project for basic research PEVE-NTUA-2010/65187900 and Alexandros S. Onassis Public Benefit Foundation for the support of this work.

## References

- [1] M.O. Aboelfotoh, A.D. Marwick, J.L. Freeouf, Phys. Rev. B., Condens. Matter. **49**, 10753 (1994)
- [2] A.E. Dolbak, B.Z. Olshanetsky, S.A. Teys, Surf. Sci. **373**, 43 (1997),
- [3] M.J. Pollard, B.A. Weinstock, T.E. Bitterwolf, P.R. Griffiths, A.P. Newbery and J.B. Paine, J. Catal. **254**, 218 (2008).
- [4] Y. Ikedo, J. Sugiyama, H. Nozaki, H. Itahara, J.H. Brewer, E.J. Ansaldo, G.D. Morris, D. Andreica A. Amato, Phys. Rev. B: Condens. Matter. **75**, 054424 (2007).
- [5] C. G. Granqvist, Handbook of Inorganic Electrochromic Materials (Elsevier, Amsterdam 1995).

- [6] M. Ando, T. Kobayashi, S. Iijima and M.J. Haruta, *Mater. Chem.* **7**, 1779 (1997).
- [7] A.U. Mane, K. Shalini and S.A. Shivashankar, *J. Phys. IV*, **11**, Pr3-63 (2001).
- [8] N.D. Papadopoulos, P.E. Tsakiridis, E. Hristoforou, *J. Optoelectron. Adv. Mater.* **7**, 2693 (2005).
- [9] R. Vladioiu, C.P. Lungu, I. Mustata, V. Bursikova, J. Bursik, *J. Optoelectron. Adv. Mater.* **9**, 1087 (2007)
- [10] E.P. Koumoulos, C.A. Charitidis, N.M. Daniolos, D.I. Pantelis, *Mater Sci Eng B* **176**, 1585 (2011).
- [11] C.A. Schuh, *Materials Today* **9**, 32 (2006).
- [12] N.D. Papadopoulos, H.S. Karayianni, P.E. Tsakiridis, E. Sarantopoulou and E. Hristoforou, *Chem. Vap. Deposition* (2011), In Press.
- [13] N.D. Papadopoulos, H.S. Karayianni, P.E. Tsakiridis, M. Perraki, E. Sarantopoulou and E. Hristoforou, *J. Electrochem. Soc.* **158**, 5 (2011); N.D. Papadopoulos, E. Illekova, H.S. Karayanni, E. Hristoforou, *J. Optoelectron. Adv. Mater.* **10**, 1098 (2008).
- [14] N.D. Papadopoulos, H.S. Karayianni, P.E. Tsakiridis, M. Perraki, E. Hristoforou, *Appl. Organomet. Chem.* **24**, 112 (2010).
- [15] T.H. Fang, W.J. Chang, C.M. Lin, *Microelectron. Eng.* **77**, 389 (2005).
- [16] S.J. Bull, *J. Phys. D: Appl. Phys.* **38**, R393 (2005).
- [17] V. Domnich, Y. Gogotsi, *Rev. Adv. Mater. Sci.* **3**, 1 (2002).
- [18] W.C. Oliver, G.M. Pharr, *J. Mater. Res.* **7**, 1564 (1992); J. Menčík, L. Beneš, *J. Optoelectron. Adv. Mater.* **10**, 3288 (2008).
- [19] I.N. Sneddon, *Proc. Cambridge Phil. Soc.* **44**, 492 (1948).
- [20] Y. Liu, A.H.W. Ngan, *Scripta Mater.* **44**, 237 (2001).
- [21] S. Lucas, J. Chevallier, *Surf. Coat. Tech.* **65**, 128 (1994).
- [22] S. Graça, R. Colaço, R. Vilar, *Surf. Coat. Tech.* **202**, 538 (2007).
- [23] Y.-T. Chen, S.R. Jian, *J. Alloy Compd.* **481**, 365 (2009).
- [24] L. Chang and L. Zhang, *Mat. Sci. Eng. A*, **506**, 125 (2009).
- [25] Y.-T. Chen, C.-M. Cheng, *Appl. Phys. Lett.* **73**, 614 (1998).
- [26] J.A. Greenwood, J.B.P. Williamson, *Proc. Roy. Soc. Lond., Ser. A, Mathem. Phys. Sci.* **295**, 300 (1966).
- [27] C.-M. Cheng, Y.-T. Chen, *Appl. Phys. Lett.* **71**, 2623 (1997).

---

\*Corresponding author: charitidis@chemeng.ntua.gr